Effect of cold clouds on satellite measurements near 183 GHz

Thomas J. Greenwald
Cooperative Institute for Research in the Atmosphere, Colorado State University, Fort Collins, Colorado, USA

Sundar A. Christopher
Institute for Atmospheric Sciences, University of Alabama, Huntsville, Alabama, USA

Received 13 December 2000; revised 31 July 2001; accepted 3 October 2001; published 9 July 2002.

[1] Near-global analysis of 183 GHz measurements from the NOAA-15 advanced microwave sounding unit (AMSU) B was conducted to investigate the impact of cold (< 240 K at 11 μm) clouds on upper tropospheric humidity (UTH) observations and in assessing the potential for deriving cloud microphysical properties. Collocated advanced very high resolution radiometer (AVHRR) data aided in identifying clouds and isolating the ice-cloud-scattering effect. This effect was determined by subtracting the measured AMSU-B brightness temperature (T_b) from a background T_b estimated using AVHRR-derived cloud optical depth data. Results for December 1999 over land and ocean show that nonprecipitating cold clouds have a measurable impact on 183 GHz T_bs although the average effect is rather weak (1.4 K). Cold clouds associated with precipitation had a much larger average effect (7 K); therefore only for these types of clouds is there sufficient information for potential quantitative estimation of cloud/precipitation physical properties. Nonprecipitating cold clouds bias estimates of UTH, on average, by 5% but can reach 20% for optically thick clouds. Precipitating clouds produce an 18% average bias. On the basis of these results it is recommended that UTH retrievals undergo filtering for precipitation (using combined microwave and infrared window channels) as well as for optically thick nonprecipitating cold clouds that fill a sensor's field of view, which may be screened using infrared split window techniques. *INDEX TERMS:* 3354 Meteorology and Atmospheric Dynamics: Precipitation (1854); 3359 Meteorology and Atmospheric Dynamics: Radiative processes; 3360 Meteorology and Atmospheric Dynamics: Remote sensing; *KEYWORDS:* microwave remote sensing, ice cloud scattering

1. Introduction

[2] The key advantage of sensing atmospheric water vapor at microwave wavelengths is the unique ability to penetrate clouds. Measurements near the 183.3 GHz water vapor absorption line are most commonly used to obtain vertical profiles of atmospheric humidity [e.g., *Wilheit*, 1990; *Engelen and Stephens*, 1999]. These measurements are also gaining popularity in estimating upper tropospheric relative humidity (UTH), a quantity most often estimated from infrared satellite measurements [e.g., *Soden and Bretherton*, 1993] which may be useful in global climate studies [*Spencer and Braswell*, 1997].

[3] It has been recognized, however, that microwave satellite measurements at these frequencies are not entirely transparent to clouds [*Engelen and Stephens*, 1998]; consequently, there have been recent efforts to develop cloud-screening methods for UTH retrievals [*Berg et al.*, 1999]. The greatest impact on these measurements is from cold clouds. Composed mostly of ice particles, they modify the upwelling radiation by scattering photons away from the satellite sensor's field of view (FOV), hence causing a brightness temperature depression. This fact has led to the development of methods for estimating ice cloud physical properties using satellite and airborne measurements near 183 GHz and in nearby "window" frequencies at 150 and 220 GHz [*Weng et al.*, 1997; *Liu and Curry*, 1998; *Deeter and Evans*, 2000].

[4] While much has been learned from simulation studies [*Wilheit*, 1990; *Muller et al.*, 1994] and limited airborne studies [e.g., *Wang et al.*, 1997, 1998] on the effect of clouds on measurements near 183 GHz, there has lacked a comprehensive effort to determine the observed effects on satellite measurements across large areas and over a wide range of atmospheric conditions. The purpose of this study is to interpret and quantify these effects using near-global data from the new advanced microwave sounding unit (AMSU). From these observations we can assess the overall potential for estimating ice cloud physical properties from satellite measurements at these frequencies and explore the implications that these cloud effects have for humidity estimates in the upper troposphere.

2. Data

[5] AMSU is the latest, most advanced set of water vapor and temperature sounding instruments. It was first launched 13 May 1998 on the NOAA-15 satellite and currently flies on

0148-0227/02/2000JD000258$09.00

Table 1. Cloud Liquid Water Sensitivity Analysis for 182.3 GHz Brightness Temperatures at Different Atmospheric Levels and for Two Different Profiles[a]

	Tropical			Midlatitude Summer		
Height, km	T_a, K	ΔT_b, K	ΔT_b, K	T_a, K	ΔT_b, K	ΔT_b, K
11	230	0.67	0.51	229	0.68	0.51
10	237	0.30	0.17	235	0.34	0.20
9	244	0.10	0.04	242	0.12	0.05
8	250	0.03	0.007	248	0.04	0.009
7	257	0.007	0.0006	255	0.009	0.0009
6	264	0.0008	0.00003	261	0.002	0.00005

[a] T_a is the atmospheric temperature and ΔT_b is the brightness temperature change relative to saturated conditions for nadir viewing (left column) and zenith angle of 58° (right column).

both NOAA-15 and NOAA-16 satellites. AMSU scans across the track of the satellite. It consists of AMSU-A (actually two separate modules) and AMSU-B. AMSU-A provides temperature soundings (50.3–57.3 GHz) and has additional channels at 23.8, 31.4, and 89 GHz. AMSU-B is devoted to moisture sounding with channels at 89, 150, 183.3 ± 1, 183.3 ± 3, and 183.3 ± 7 GHz. The latter three channels consist of pairs of narrow passbands on either side of the H_2O absorption line center. For the channel of interest here (183.3 ± 1 GHz), the temperature sensitivity is 1.1 K and the calibration is known to within about ±1 K. All channels of AMSU-B have a spatial resolution of 16 km at nadir. Footprint size increases to about 34 × 52 km at the limb.

[6] Throughout its early history, AMSU-B unfortunately suffered from radio frequency interference (RFI) via one of the onboard data transmitters due to improper shielding of the instrument. This resulted in much of the early data for most of the channels to be unusable. This problem has since been resolved, however. The data used in this study do not suffer from RFI.

[7] The advanced very high resolution radiometer (AVHRR), which also flies on NOAA-15, is a visible/IR instrument used here to derive cloud physical properties and to characterize cloud conditions within the field of view of AMSU-B. AVHRR is a five-channel cross-track scanning instrument with central wavelengths at 0.63, 0.91, 3.74, 10.8, and 12.0 μm. This study uses the global area coverage (i.e., 4 × 4 km resolution) data.

3. Analysis Approach

[8] Because our goal is to isolate the scattering signature of cold clouds, we selected the AMSU-B 183 ± 1 GHz data because they are closest to the absorption line center where the weighting function peaks in the upper troposphere (typically about 300–400 mbar, depending on the atmospheric conditions). The advantage of these measurements over those in nearby wings of the absorption line is that the ground surface and liquid water clouds in the lower to the middle troposphere have a negligible impact [e.g., *Muller et al.*, 1994]. The exception occurs in drier atmospheres and higher altitudes where the surface can contribute significantly to the measured brightness temperature; however, these conditions are excluded from our analysis.

[9] "Cold" clouds are defined here as having an equivalent blackbody (EBB) temperature of less than 240 K from window IR (10.8 μm) AVHRR measurements. This is to ensure they are composed primarily of ice particles. Studies have indicated that supercooled liquid water may exist even under these conditions [e.g., *Sassen*, 1985]. To address the possibility of emission effects from liquid water droplets, we performed calculations for climatological midlatitude summer and tropical profiles and inserted a liquid water content of 0.02 gm^{-3} (a value greater than measured) at various levels in the profiles. The results are expressed relative to saturated air (relative humidity of 100%). They show that the change in brightness temperature is negligible (< 1 K), well within the noise level of the instrument (see Table 1). The explanation is that although the liquid water absorption coefficient is very large (because it increases with frequency and decreasing temperature), there is simply insufficient mass to compete radiatively with the extremely large water vapor absorption. Therefore we conclude that at least for nonprecipitating clouds, scattering processes are the primary contributor to the observed cloud effect. The same may not be said for precipitating systems however, where emission by cloud droplets can also influence the measured brightness temperature [e.g., *Smith et al.*, 1992].

[10] We define the scattering signal as a brightness temperature depression,

$$\Delta T_b = T_{\mathrm{bkg}} - T_{\mathrm{meas}},$$

following *Evans and Stephens* [1995], where T_{bkg} is a background brightness temperature under saturated clear-sky conditions, and T_{meas} is the measured brightness temperature. Our approach for estimating T_{bkg} is to take advantage of estimates of cloud visible optical depth derived from the AVHRR. An example of how this is done is illustrated in Figure 1. The idea is that ice clouds of increasing optical depth, which presumably contain greater ice water mass, will generally have increasing brightness temperature depressions (i.e., ΔT_b) at 183 GHz. Thus by plotting the AMSU-B measurements (for strictly nonprecipitating clouds) versus the AVHRR-derived optical depth over a given region, one can compute a least squares fit line and then extrapolate the relationship to zero optical depth, where the corresponding brightness temperature is T_{bkg}. Applying a linear fit is valid because radiative transfer is linear at these optical depths and at this frequency [*Evans and Stephens*, 1995].

[11] Our approach for deriving ice cloud properties from solar reflectance measurements is to use two measurements to simultaneously retrieve optical depth and mean particle size. One of these measurements is at a relatively nonabsorbing visible wavelength that is mostly sensitive to optical depth, while the other is at a near-infrared wavelength (outside of molecular absorption lines) which is mostly sensitive to changes in particle size. This type of

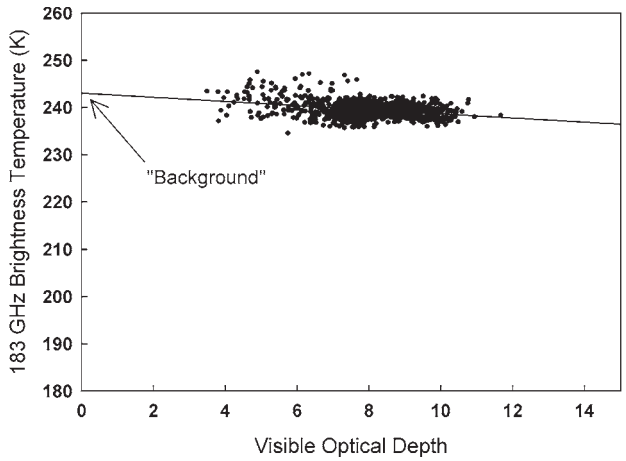

Figure 1. Illustration of method for estimating background 183 GHz brightness temperature using AMSU-B measurements (vertical axis) and AVHRR-derived cloud visible optical depth (horizontal axis) for overcast, nonprecipitating cold clouds.

approach has been used often in retrieving liquid water cloud and ice cloud physical properties [e.g., *Nakajima et al.*, 1991; *Minnis et al.*, 1998; *Greenwald and Christopher*, 2000]. Recently, *Young et al.* [1998] demonstrated the validity of optical depth and particle size retrievals of ice clouds from the AVHRR using a similar method through detailed comparisons to in situ aircraft measurements.

[12] Specifically, our approach is to first generate a set of tables of reflectances for the AVHRR visible channel (0.63 μm) and near-IR channel (3.74 μm) for a range of cloud optical depths, particle sizes, solar geometry, and instrument viewing angles. A discrete ordinate radiative transfer model was used to compute reflectances, while single-scattering cloud properties were derived from Lorenz-Mie Theory. Ice particles were modeled as equivalent area ice spheres, and a gamma size distribution was assumed. We recognize that assuming ice particles to be equivalent area spheres has been shown to be inadequate for radiative transfer through realistic ice clouds, which are composed of different particle shapes and sizes. This is not a major issue here because our main interest is in the retrieved optical depth, for which accurate knowledge of particle size and shape is not so crucial. Before proceeding with the retrieval, we removed the thermal emission component from the AVHRR near-IR measurements using the approach of *Allen et al.* [1990]. The retrieval process itself uses the appropriate table (given the solar and instrument geometry) and two reflectance measurements to interpolate a bispectral grid (i.e., visible reflectance versus near-IR reflectance) to yield a unique value for the optical depth and particle-effective radius. An example of AVHRR retrievals for cold clouds for one NOAA-15 orbit is shown in Figure 2.

[13] An important aspect of the analysis is discriminating between cold clouds that are associated with precipitation and those that are not. The precipitation detection algorithm used here is currently being implemented for Day-2 precipitation products provided by the National Oceanic and Atmospheric Administration/National Environmental Satellite Data and Information Service (NOAA/NESDIS). Briefly, it is a scattering-type method based mainly on the AMSU-B 89 GHz and 150 GHz channels (see Appendix A for details). Tests of this new method for several case studies have produced highly favorable results (N. Grody, personal communication, 2000). Our own analysis has shown that the method provides reasonable geographic distributions of precipitation frequency. For example, in Figure 3 the frequency of occurrence of precipitating versus nonprecipitating cold clouds for December 1999 shows, as one might expect, a strong precipitation peak in the tropics associated with deep convection but which falls off rapidly toward higher latitudes (note that the unusually rapid decline north of about 15°N is due in part to our restriction on the AVHRR cloud optical depth retrievals). Nonprecipitating cold clouds, in contrast, are shown to be more numerous at higher latitudes, particularly south of 45°S, which is another expected result. We therefore conclude that the precipitation detection algorithm appears to behave well qualitatively at least under cold cloud conditions.

[14] Before proceeding with the analysis, however, the effect of limb darkening on the AMSU-B measurements must be addressed. This is important because limb darken-

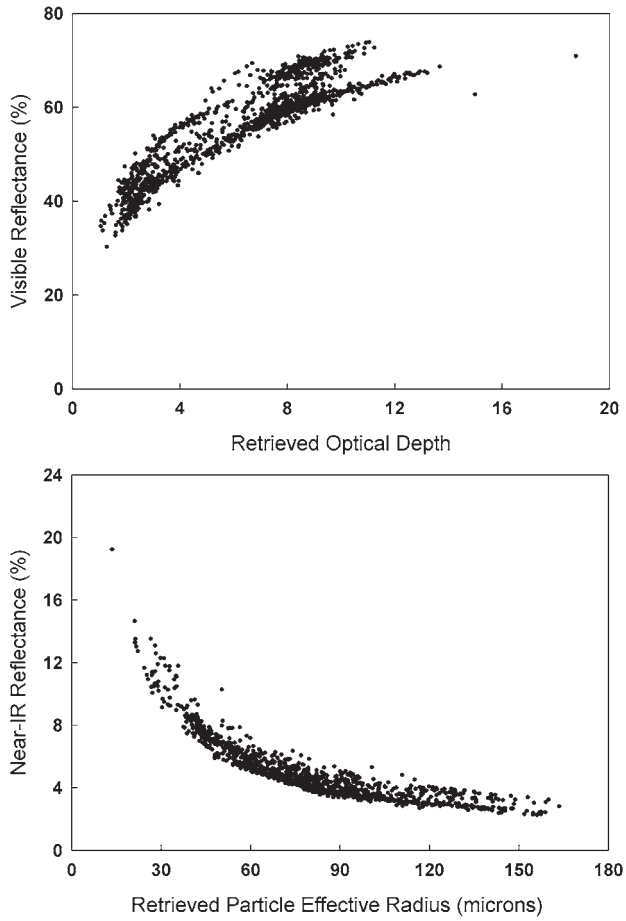

Figure 2. AVHRR (top) visible channel (0.65 μm) measurements versus retrievals of cloud optical depth and (bottom) near-infrared (3.7 μm) reflectance observations versus particle-effective radius for cold, overcast clouds on 1 December 1999 for NOAA-15 orbit starting at 0459 UT.

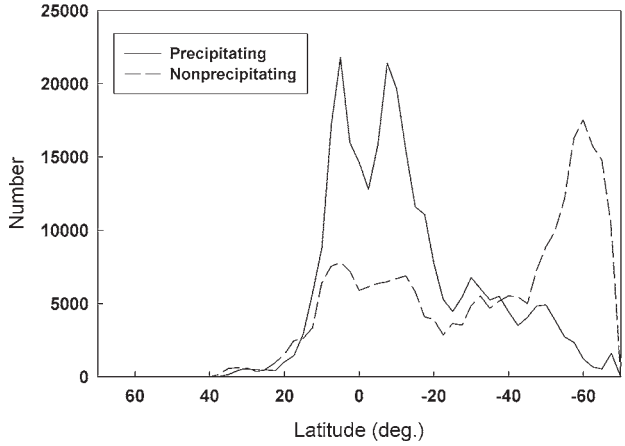

Figure 3. Latitudinal distribution of precipitating and nonprecipitating cold clouds for December 1999 limited to daytime and cloud-filled AMSU-B fields of view.

ing is of the same order as the scattering signal we are seeking. This analysis was limited to cold, nonprecipitating clouds for overcast AMSU-B field of views, as determined by the AVHRR. Grouping the data as a function of the AMSU-B beam position reveals the expected limb darkening, which can approach 5 K at the largest angles (see Figure 4). This phenomenon occurs because at larger zenith angles the 183 GHz weighting function peaks at a higher altitude, hence colder temperature. We stress that the limb-darkening effect observed in Figure 4 would not have been possible without the aid of coincident visible/IR data. All overcast AMSU-B data were corrected for limb darkening.

[15] December 1999 was selected for the analysis. The first step was to collocate AVHRR measurements with AMSU-B data. This was done by collecting all AVHRR pixels within the FOV of AMSU-B while accounting for spreading out of the AMSU-B footprint with increasing viewing angle. In this collocation method we assume that the navigation for both AMSU-B and AVHRR is reasonably accurate. The analysis was limited to 67°N to 67°S for the purpose of minimizing surface snow and ice effects, whose high reflectivity can introduce large errors in the AVHRR retrievals. An operational algorithm to detect surface snow/ice using AMSU-A and AMSU-B data (see Appendix A) was also used to eliminate these cases if they occurred. AVHRR retrievals were limited to daytime conditions with a solar zenith angle of less than 75° because retrievals are less reliable for low Sun angles. Since visible optical depth retrievals are also less reliable for optically thin cirrus clouds, these conditions were detected and eliminated using brightness temperature differences between AVHRR split window channels [*Inoue*, 1987].

[16] The procedure for estimating T_{bkg} was to collect data for overcast, cold clouds (which also met other criteria described above) into $10^\circ \times 10^\circ$ regions for each satellite orbit. The reason for selecting such large regions was that it greatly increased the opportunities for estimating T_{bkg}. Through trial and error it was found that at least 80 data points in each region were needed to provide a reasonable fit through the AMSU-B brightness temperature and optical depth data for nonprecipitating conditions. Use of smaller grid spacing, however, did not significantly change the overall results but did greatly reduce the number of regions where a regression analysis was possible. Of course, using rather large regions for the analysis has its drawbacks. For example, the assumption that T_{bkg} is constant over $10^\circ \times 10^\circ$ regions may be questionable, and there is the possibility of introducing large discontinuities at the grid boundaries. However, T_{bkg} was found to be remarkably stable from region to region with an overall mean and standard deviation of 241.9 ± 2.1 K.

4. Results

[17] Instantaneous estimates of ΔT_b over land and ocean for December 1999 were separated into precipitating and nonprecipitating conditions and presented as histograms (Figure 5). To reiterate, these results are only for overcast AMSU-B FOVs containing cold clouds. FOVs with partial/broken cloudiness will have only a negligible impact on the AMSU-B measurements. The histograms show there is only a somewhat greater occurrence of nonprecipitating clouds than precipitating. This is because the analysis is biased toward regions in and around precipitation where the cloud cover is usually more extensive, which increases the chan-

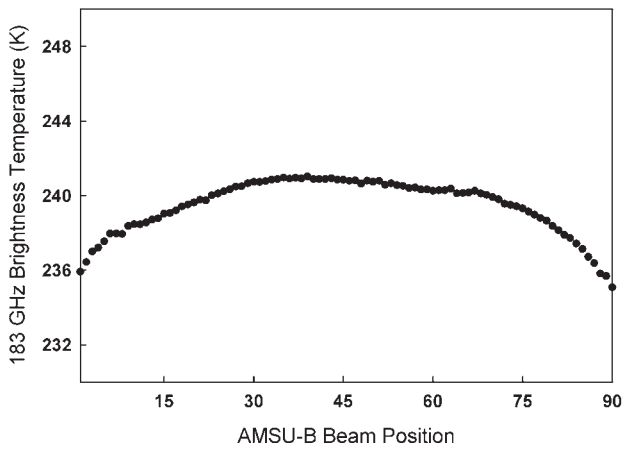

Figure 4. Depiction of limb-darkening effect for overcast, nonprecipitating AMSU-B fields of view containing cold clouds in December 1999.

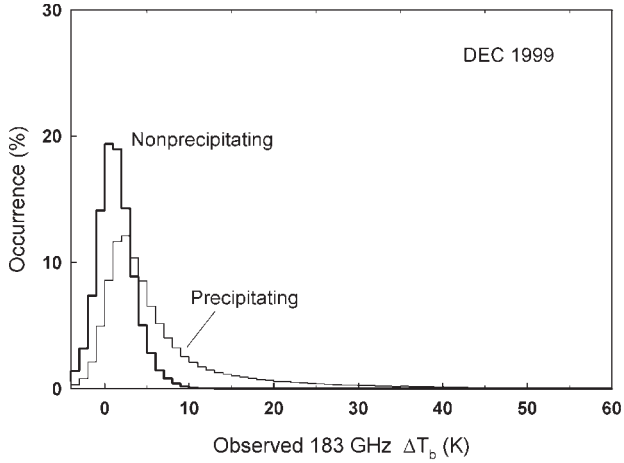

Figure 5. Number histograms of scattering effect (ΔT_b) measured by the AMSU-B 183 ± 1 channel for nonprecipitating and precipitating cold clouds in December 1999.

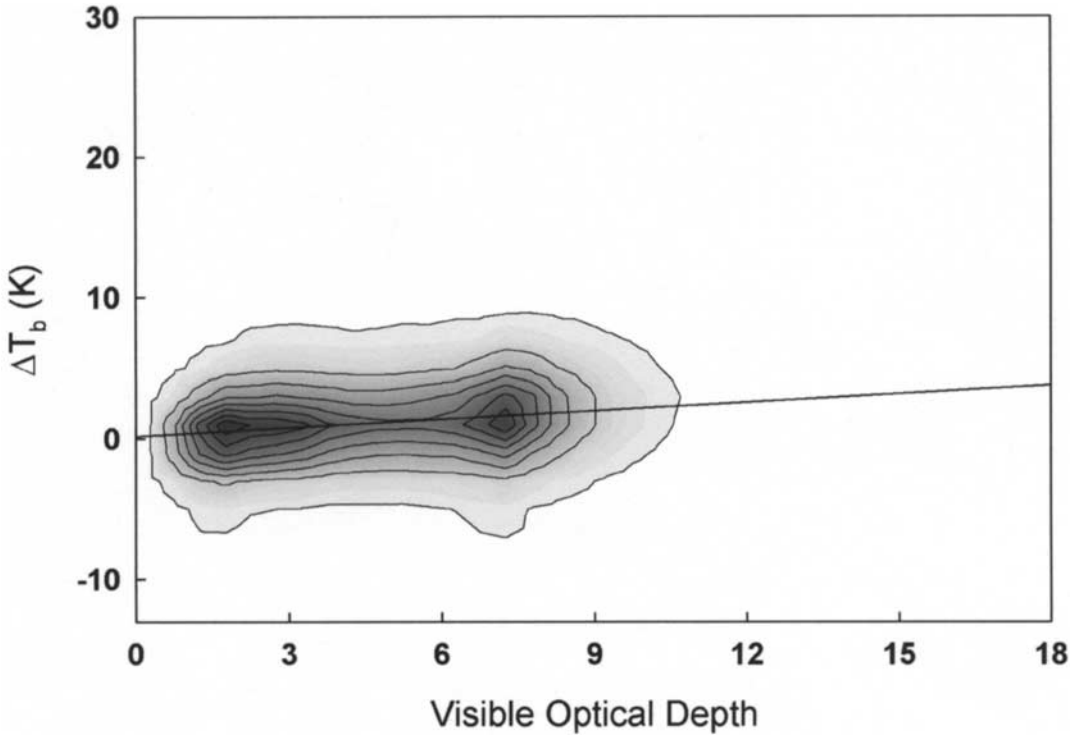

Figure 6. AMSU-B-observed scattering effect (ΔT_b) versus visible optical depth for cold, nonprecipitating clouds in December 1999 represented as a 2-D frequency of occurrence histogram where darker shades are greater occurrences. Also shown is the least squares fit line.

ces of determining a background microwave brightness temperature.

[18] In Figure 5 also notice there is significant overlap of both histograms for small ΔT_b. We suspect there may be two possible reasons for this behavior. One, the precipitation detection (PD) algorithm may be producing false hits (i.e., detecting precipitation where none is occurring). Tests of the sensitivity of the PD algorithm showed that it was not overly sensitive to moderate changes made to the brightness temperature thresholds used. Another more likely possibility is that the AMSU-B window channels (89 and 150 GHz) used for detecting precipitation respond differently to precipitation than the 183 ± 1 GHz channel. Being window channels, they can peer somewhat deeper inside the cloud, which implies that hydrometeor vertical structure, to a certain extent, plays a role in the interpretation of these measurements. This may explain why, from the perspective of the window channels, that precipitation is occurring, while little or no signature is seen in the 183 ± 1 GHz measurements.

[19] For nonprecipitating clouds the most notable feature is that the distribution is slightly skewed. This suggests that some of the clouds produce a measurable impact on the AMSU-B data. If all clouds were completely transparent, then one would expect a Gaussian-like distribution centered about zero. On average, these clouds produce a 1.4 K depression, which is roughly at the threshold of detectability of the instrument. When ΔT_b is plotted against optical depth for nonprecipitating conditions (Figure 6), a small positive relationship emerges. However, the overall relationship is very weak (0.21 K per unit optical depth) and shows that even the optically thickest nonprecipitating cold clouds will only impact the measurements, on average, by about 2.5 K. The somewhat large scatter (2.4 K root-mean-square (RMS)) suggests that other factors may be at play in the relationship between ΔT_b and optical depth, such as particle size [e.g., *Evans and Stephens*, 1995]. Other errors due to scene misidentification, satellite navigation, instrument noise, optical depth retrievals, and errors in T_{bkg} contribute additional uncertainty to this relationship. These results demonstrate that the 183 GHz scattering signature is in fact measurable for nonprecipitating clouds but is generally too small for providing quantitative cloud property information.

[20] For precipitating cold clouds the mode of the distribution is shifted slightly to the right and the distribution has a much longer tail. The average ΔT_b increases to 6.8 K, indicating greater potential for inferring precipitation physical properties from these measurements. The geographic distribution of ΔT_b is depicted in Figure 7. Note that the lack of data in much of the Northern Hemisphere is the result of the Sun angles being too low to perform reliable optical depth retrievals. The largest values of ΔT_b occur in regions associated with intense tropical convection and, to a lesser extent, in the midlatitude storm tracks. These values can exceed 20 K but are somewhat rare, occurring about 8% of the time. In one extreme case, ΔT_b was nearly 120 K.

[21] The overall effects of cold clouds on 183 GHz brightness temperatures can be viewed by combining the results for both precipitating and nonprecipitating clouds and displaying them as a function of latitude. In Figure 8 we find that the zonally averaged ΔT_b can reach 7 K in the tropics but is under 1 K south of about 50°S because of the predominance of nonprecipitating cold clouds.

[22] What effects will these clouds have on retrievals of UTH? To address this question quantitatively, we used the

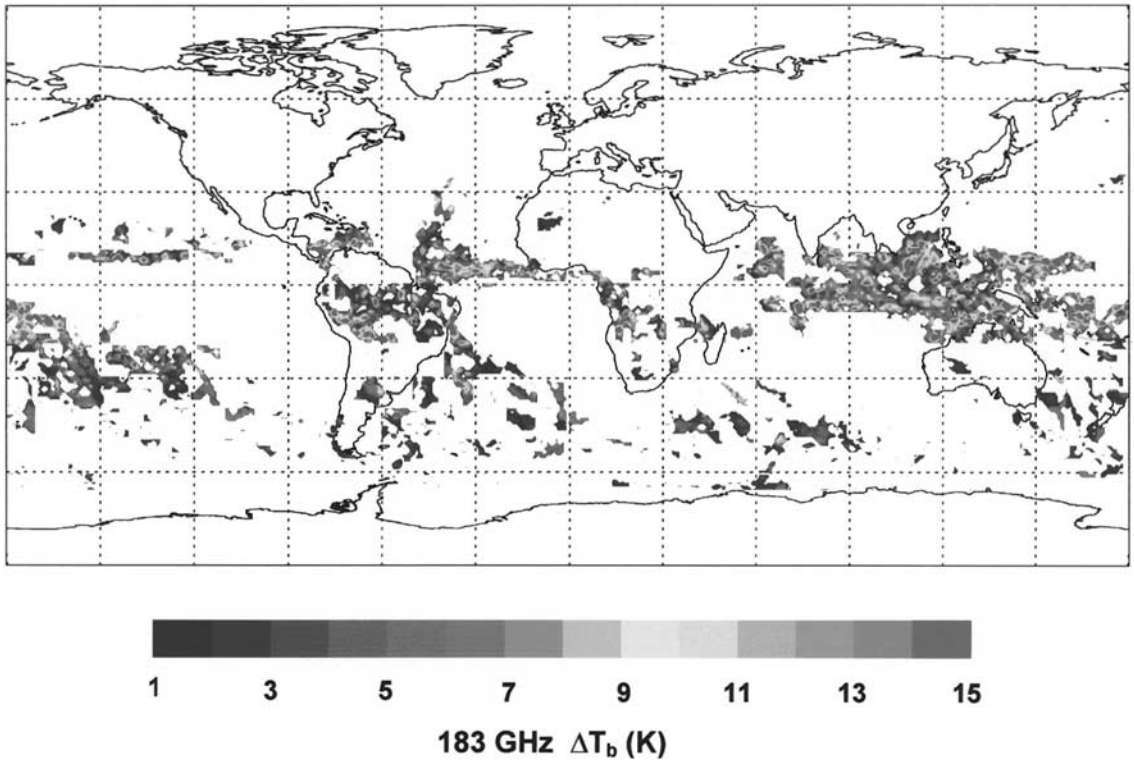

Figure 7. Spatial pattern of 183 GHz ΔT_b for precipitating cold clouds on a 1° grid for December 1999. See color version of this figure at back of this issue.

following simplified relationship between UTH and brightness temperature (T_b) [*Soden and Bretherton*, 1996]:

$$\mathrm{UTH} = \frac{\exp(a + bT_b)}{p_o}, \qquad (1)$$

where the fit coefficients are $a = 20.95$ and $b = -0.089$, which were derived from more detailed radiative transfer calculations [*Engelen and Stephens*, 1998], and p_o is a normalized reference pressure (equal to the pressure of the 240 K isotherm divided by 300 mbar). Equation (1) differs slightly from the expression of *Soden and Bretherton* [1996] in that the zenith angle factor is missing. This is because the AMSU-B brightness temperatures have already been corrected to nadir-viewing conditions, as discussed earlier. The normalized reference pressure varies seasonally and regionally [*Soden and Bretherton*, 1996]. Thus we used climatic values of p_o for December as a function of latitude determined from the European Centre for Medium-Range Weather Forecast (ECMWF) analyses. Equation (1) was applied to both the derived background T_b and the AMSU-B measured T_b. This difference (in terms of absolute %) was the estimated error in UTH.

[23] The results of this error analysis are shown in Figure 9. On average, nonprecipitating cold clouds cause

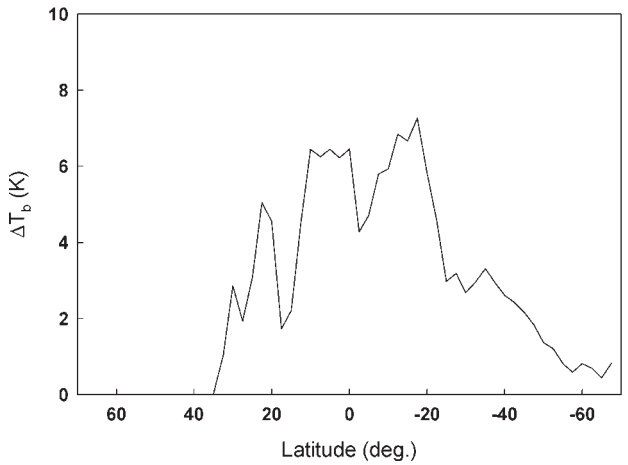

Figure 8. Total scattering effect (ΔT_b) as a function of latitude for clouds in December 1999.

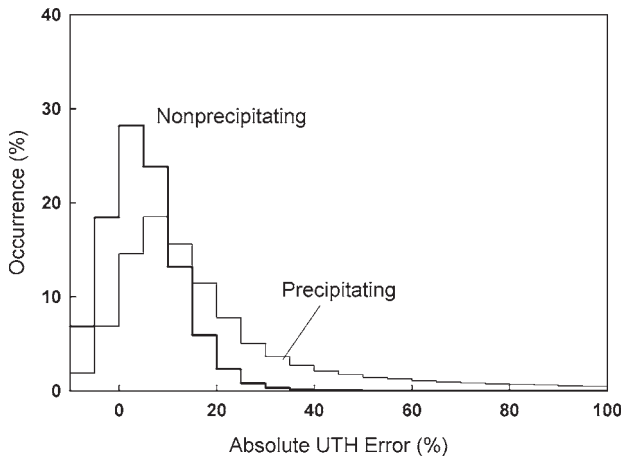

Figure 9. Frequency of occurrence of absolute errors in upper tropospheric relative humidity (UTH) observations for precipitating and nonprecipitating conditions for the same data shown in Figure 5.

an overestimation of UTH by 5.1%. This systematic error is of the order of the variability in the relationship given in (1) between UTH and T_b [*Engelen and Stephens 1998*], which is attributed to unmodeled effects. Therefore, on average, these clouds do not have an appreciable effect on UTH retrievals. However, optically thick clouds may bias the UTH by up to 20%. In the case of precipitating clouds the effects are much larger, on average, overestimating the UTH by 18%.

5. Conclusions and Recommendations

[24] An in-depth analysis of 183 GHz satellite measurements using collocated AMSU-B and AVHRR data was done to isolate, quantify, and interpret the scattering signatures of cold clouds over land and ocean from 67°N to 67°S. We emphasize that quantifying these signatures would not have been possible without the aid of visible/IR data, in this case the AVHRR. While it is commonly thought that ''all'' nonprecipitating ice clouds have a negligible effect on 183 GHz brightness temperatures (i.e. within instrument noise levels), our results indicate that this is only partially true. Rather, these clouds do, in fact, have a measurable impact although the signal is quite small (1.4 K, on average). Consequently, these measurements have little or no potential for estimating quantitative cloud physical property information. Studies that claim to provide quantitative satellite estimates of physical properties of nonprecipitating cold clouds using microwave frequencies at or below 183 GHz are highly questionable. The results of this work support the use of even higher microwave frequencies for deriving ice cloud properties, as suggested by earlier observational and theoretical studies [*Evans et al.*, 1998; *Weng and Grody*, 2000].

[25] Because of larger signatures, measurements of precipitating cold clouds afford a greater chance of providing quantitative information concerning properties of large hydrometeors. Under these conditions, the scattering signature was, on average, 6.8 K. However, it is somewhat difficult to relate this signature directly to physical properties, such as ice water path, since it is also a function of particle size [*Evans and Stephens*, 1995; *Liu and Curry*, 1998] and may depend on hydrometeor type and profile as well. Because of these potential ambiguities it might be best to treat the signature as simply a scattering index until much higher frequency microwave measurements become available.

[26] Interpretation of 183 GHz brightness temperatures in cloudy conditions also has a bearing on studies that attempt to use these data for climate monitoring of UTH [e.g., *Spencer and Braswell*, 1997]. Our results show, on average, that nonprecipitating cold clouds have an effect comparable to the inherent uncertainties in the UTH retrievals themselves. Thus it may not be necessary to filter out all clouds (as done for infrared measurements) but only the most optically thick ones that are colder than about 240 K at 11 μm. The method of *Inoue* [1987] can be used for this purpose, which takes the difference between the equivalent blackbody temperatures obtained from infrared split window channels (11 and 12 μm). Optically thicker clouds produce smaller differences, where a difference threshold of 2.5 K is recommended [*Inoue*, 1987]. Cloud-screening methods that use only microwave window channels [e.g., *Berg et al.*, 1999], which essentially apply a liquid water path (LWP) threshold, may tend to ''overscreen'' by eliminating scenes in which the LWP is large yet the clouds are relatively low in the troposphere. These cloud conditions have a negligible impact on the 183 GHz brightness temperatures and thus the data should not be filtered. Only through combined use of microwave and infrared data can these situations be detected.

[27] Cold clouds associated with precipitation were found to have the largest impact on UTH retrievals. On average, they introduced a bias error of 18%. Microwave window measurements are ideally suited for detecting precipitation. However, these measurements should be accompanied by window infrared measurements to identify cold clouds. Applying thresholds to UTH retrievals in order to filter clouds and precipitation [e.g., *Engelen and Stephens*, 1998] is usually inadequate since they do not eliminate optically thick clouds and all precipitation events. We anticipate that the new dual-sensor strategy proposed here for screening precipitation and unwanted clouds will maximize the utility of UTH data in regional and global climate studies.

Appendix A

[28] The rain detection algorithm that uses primarily AMSU-B data is a scattering-based technique that is separated into two algorithms, one for land and one for water. Over land, a scattering index (P) is computed as

$$P = 44.96 + 0.85T_{b,89} - T_{b,150},$$

where $T_{b,89}$ is the AMSU-B brightness temperature at 89 GHz and $T_{b,150}$ is the brightness temperature at 150 GHz. A first-level test triggers rain if $P > 8$. Second-level criteria for testing whether rain is unlikely is for AMSU-A 23.8 GHz brightness temperature ($T_{b,23.8}$) $\leq$ 264 K or $T_{b,23.8} \geq 260$ K and $T_{b,150} \geq T_{b,89}$. There are additional checks for anomalous signatures due to snow ($T_{b,23.8} < 260$ K) and desert ($T_{b,183\pm3} - T_{b,89} \geq 0$ K).

[29] Over water surfaces, P has a different form and is computed only when $T_{b,150} < 295$ K:

$$P = T_{b,89} + a_2 \ln(300 - T_{b,150}) - a_o,$$

where

$$a_o = b_o - a_1 \cos(\theta),$$

where θ is the sensor viewing angle. The coefficients b_o, a_1, and a_2 depend on the beam position (1–90). For positions ≤ 11, $b_o = 354.10$, $a_1 = 6.073$, and $a_2 = 33.20$; for positions between 11 and 85, $b_o = 348.07$, $a_1 = 21.58$, and $a_2 = 29.06$; and for positions ≥ 85, $b_o = 357.89$, $a_1 = 11.15$, and $a_2 = 34.136$. Rainfall is triggered when $P > 25$ (note that in this study we assumed a slightly more conservative threshold of 28 based on inspection of the overall bimodal distribution of P).

[30] **Acknowledgments.** Financial support was provided by the DoD Center for Geosciences Atmospheric Research agreement DAAL01-98-2-0078. S. Christopher was supported by NASA grant NAGW-5195. We

thank J. Chou for her work on the AVHRR retrievals, R. Engelen for supplying the UTH fit coefficients, and N. Grody for supplying the AMSU-B precipitation detection algorithm. We also appreciate the work of the CIRA infrastructure group in processing the AVHRR data.

References

Allen, R. C., Jr., P. A. Durkee, and C. H. Wash, Snow/cloud discrimination with multispectral satellite measurements, *J. Appl. Meteorol.*, *29*, 994–1004, 1990.

Berg, W., J. J. Bates, and D. L. Jackson, Analysis of upper-tropospheric water vapor brightness temperatures from SSM/T-2, HIRS, and GMS-5 VISSR, *J. Appl. Meteorol.*, *38*, 580–595, 1999.

Deeter, M. N., and K. F. Evans, A novel ice-cloud retrieval algorithm based on the millimeter-wave imaging radiometer (MIR) 150- and 220-GHz channels, *J. Appl. Meteorol.*, *39*, 623–633, 2000.

Engelen, R. J., and G. L. Stephens, Comparison between TOVS/HIRS and SSM/T-2-derived upper-tropospheric humidity, *Bull. Am. Meteorol. Soc.*, *79*, 2748–2751, 1998.

Engelen, R. J., and G. L. Stephens, Characterization of water-vapour retrievals from TOVS/HIRS and SSM/T-2 measurements, *Q. J. R. Meteorol. Soc.*, *125*, 331–351, 1999.

Evans, K. F., and G. L. Stephens, Microwave radiative transfer through clouds composed of realistically shaped ice crystals, part II, Remote sensing of ice clouds, *J. Atmos. Sci.*, *52*, 2058–2072, 1995.

Evans, K. F., S. J. Walter, A. J. Heymsfield, and M. N. Deeter, Modeling of submillimeter passive remote sensing of cirrus clouds, *J. Appl. Meteorol.*, *37*, 184–205, 1998.

Greenwald, T. J., and S. A. Christopher, The GOES I-M imagers: New tools for studying microphysical properties of boundary layer stratiform clouds, *Bull. Am. Meteorol. Soc.*, *81*, 2607–2619, 2000.

Inoue, T., A cloud-type classification with NOAA 7 split-window measurements, *J. Geophys. Res.*, *92*, 3991–4000, 1987.

Liu, G., and J. A. Curry, Remote sensing of ice water characteristics in tropical clouds using aircraft measurements, *J. Appl. Meteorol.*, *37*, 337–355, 1998.

Minnis, P., D. P. Garber, D. F. Young, R. F. Arduini, and Y. Takano, Parameterizations of reflectance and effective emittance for satellite remote sensing of cloud properties, *J. Atmos. Sci.*, *55*, 3313–3339, 1998.

Muller, B. M., H. E. Fuelberg, and X. Xiang, Simulations of the effects of water vapor, cloud liquid water, and ice on AMSU moisture channel brightness temperatures, *J. Appl. Meteorol.*, *33*, 1133–1154, 1994.

Nakajima, T., M. D. King, J. D. Spinhirne, and L. F. Radke, Determination of the optical thickness and effective particle radius of clouds from reflected solar radiation measurements, part II, Marine stratocumulus observations, *J. Atmos. Sci.*, *48*, 728–749, 1991.

Sassen, K., Highly supercooled cirrus cloud water: Confirmation and climatic implications, *Science*, *227*, 411–413, 1985.

Smith, E. A., A. Mugnai, H. J. Cooper, G. J. Tripoli, and X. Xiang, Foundations for statistical-physical precipitation retrieval from passive microwave satellite measurements, part I, Brightness temperature properties of a time dependent cloud-radiation model, *J. Appl. Meteorol.*, *31*, 506–531, 1992.

Soden, B. J., and F. P. Bretherton, Upper tropospheric humidity from the GOES 6.7 μm channel: Method and climatology for July 1987, *J. Geophys. Res.*, *98*, 16,669–16,688, 1993.

Soden, B. J., and F. P. Bretherton, Interpretation of TOVS water vapor radiances in terms of layer-average relative humidities: Method and climatology for the upper, middle, and lower troposphere, *J. Geophys. Res.*, *101*, 9333–9343, 1996.

Spencer, R. W., and W. D. Braswell, How dry is the tropical free troposphere? Implications for global warming theory, *Bull. Am. Meteorol. Soc.*, *78*, 1097–1106, 1997.

Wang, J. R., J. D. Spinhirne, P. Racette, L. A. Chang, and W. Hart, The effect of clouds on water vapor profiling from the millimeter-wave radiometric measurements, *J. Appl. Meteorol.*, *36*, 1232–1244, 1997.

Wang, J. R., P. Racette, J. D. Spinhirne, K. F. Evans, and W. D. Hart, Observations of cirrus clouds with airborne MIR, CLS, and MAS during SUCCESS, *Geophys. Res. Lett.*, *25*, 1145–1148, 1998.

Weng, F., and N. C. Grody, Retrieval of ice cloud parameters using a microwave imaging radiometer, *J. Atmos. Sci.*, *57*, 1069–1081, 2000.

Weng, F., N. C. Grody, R. R. Ferraro, Q. Zhao, and C. T. Chen, Global cloud water distribution derived from Special Sensor Microwave Imager/Sounder and its comparison with GCM simulation, *Adv. Space Res.*, *19*, 407–411, 1997.

Wilheit, T. T., An algorithm for retrieving water vapor profiles in clear and cloudy atmospheres from 183 GHz radiometric measurements: Simulation studies, *J. Appl. Meteorol.*, *29*, 508–515, 1990.

Young, D. F., P. Minnis, and D. Baumgardner, Comparison of in situ and satellite-derived cloud properties during SUCCESS, *Geophys. Res. Lett.*, *25*, 1125–1128, 1998.

S. A. Christopher, Institute for Atmospheric Sciences, University of Alabama, Huntsville, AL 35807, USA.

T. J. Greenwald, Cooperative Institute for Research in the Atmosphere (CIRA), Colorado State University, Fort Collins, CO 80523-1375, USA. (greenwald@cira.colostate.edu)

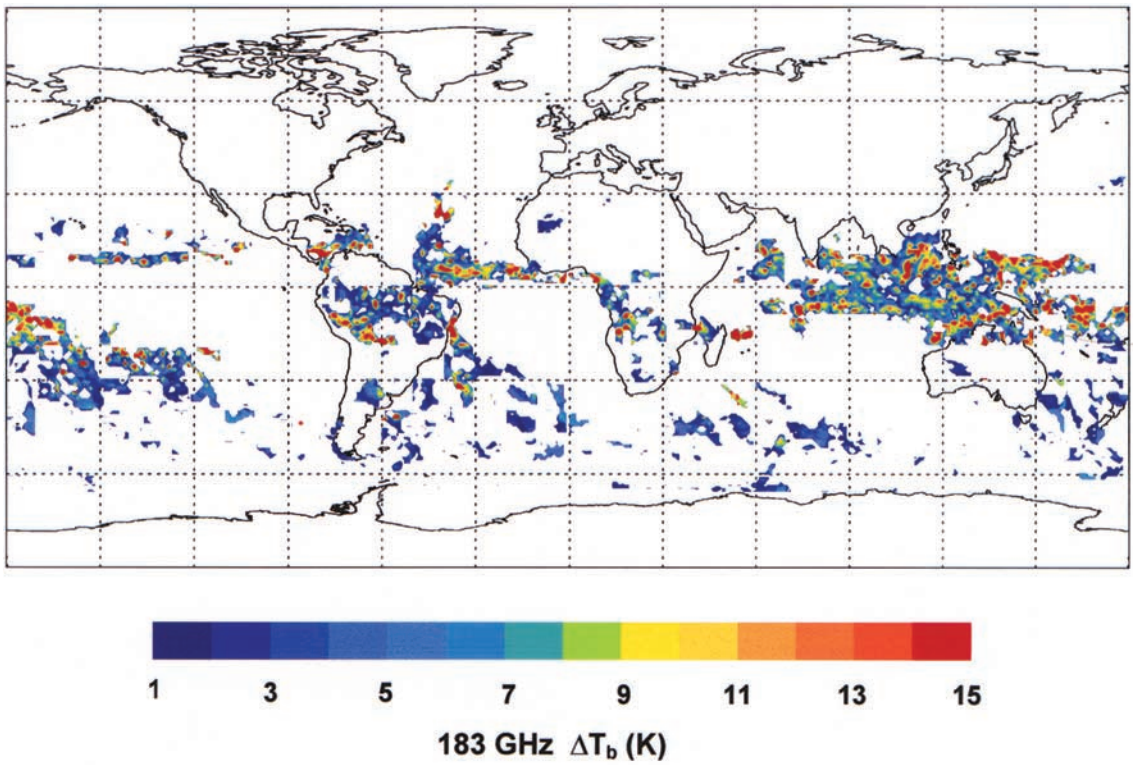

Figure 7. Spatial pattern of 183 GHz ΔT_b for precipitating cold clouds on a 1° grid for December 1999.